

COARSE-GRAINING OF TWO-FLUID MODELS FOR FLUIDIZED GAS-PARTICLE SUSPENSIONS

Yesim IGC¹, Sankaran SUNDARESAN¹, Sreekanth PANNALA², Thomas O'BRIEN³ and
 Ronald W. BREULT³

¹ Department of Chemical Engineering, Princeton University, Princeton, NJ 08544, USA

² Oak Ridge National Laboratory, Oak Ridge, TN 37831, USA

³ National Energy Technology Laboratory, Morgantown, WV 26507, USA

ABSTRACT

Gas-particle flows in fluidized beds and circulating fluidized beds are inherently unstable, and they manifest fluctuations in velocities and local suspension density over a wide range of length and time scales. In riser flows, these fluctuations are associated with the random motion of the individual particles and with the chaotic motion of particle clusters. Coarse-grid simulations for industrial scale gas-particle flows will clearly not resolve the structures which exist on sub-grid length scales; however, these small-scale unresolved structures are known to affect the resolved flow characteristics. We pursue a filtered equations approach in which the influence of the small scale structures appears as residual correlations for which constitutive models should be constructed. In our present study, we examine the filter-width dependence of correlations in the filtered two-fluid model through three-dimensional (3-D) calculations and demonstrate that the filtered drag coefficient extracted from the analysis of computational data generated through highly resolved 3-D simulations of a kinetic theory based two-fluid model decreased systematically with increasing filter width. We also show that both 2-D and 3-D simulations yield qualitatively similar results.

NOMENCLATURE

d	particle diameter
ρ_g	gas density
ρ_s	particle density
e_p	coefficient of restitution
μ_g	gas viscosity
P_g	pressure
ϕ	particle phase volume fraction
v_t	terminal settling velocity
$\underline{\underline{\sigma}}_s$	particle phase stress tensor
$\underline{\underline{\sigma}}_g$	gas phase stress tensor
\mathbf{f}	gas-particle interaction force
\mathbf{g}	gravitational acceleration
\mathbf{d}	rate of strain tensor
Ψ	filtered drag
$\underline{\underline{\Theta}}_s$	filtered particle phase stress
\mathbf{u}	local average gas velocity
\mathbf{v}	local average particle velocity
$\langle \mathbf{u} \rangle$	volume-weighted gas phase velocity

$\langle \mathbf{v} \rangle$	volume-weighted particle phase velocity
$\bar{\mathbf{u}}$	filtered (region-averaged) gas phase velocity
$\bar{\mathbf{v}}$	filtered (region-averaged) particle phase velocity
$\beta_{filtered}$	filtered drag coefficient

INTRODUCTION

Chemical reactors that take the form of fluidized beds and circulating fluidized beds are widely used in energy-related and chemical process industries. The number of particles present in most gas-particle flow systems is large, rendering detailed description of the motion of all the particles and fluid elements impractical. Hence, two-fluid model (TFM) equations [1], where the gas and particle phases are treated as inter-penetrating continua, are commonly employed. The general form of the TFM equations is fairly standard and this has permitted the development of numerical methods geared towards solving them. Open-source packages such as MFIX [2, 3] and other commercial software (e.g., Fluent[®]) can readily be applied to perform transient integration (of the discretized forms) of the TFM equations.

The Stokes number associated with the particles in many gas-particle mixtures is sufficiently large that particle-particle and particle-wall collisions do occur; furthermore, when the particle volume fraction is below ~ 0.5 , the particle-particle interactions in these systems occur largely through binary collisions. The particle phase stress in these systems is widely modelled through the kinetic theory of granular materials (e.g., see [1, 4]).

Gas-particle flows in fluidized beds and circulating fluidized beds are inherently unstable, and they manifest fluctuations in velocities and local suspension density over a wide range of length and time scales. In riser flows, these fluctuations are associated with the random motion of the individual particles (typically characterized through the granular temperature) and with the chaotic motion of particle clusters, which are repeatedly formed and broken apart. The origin of these clusters is well understood, and it is now well established that TFM equations are able to capture their existence in a robust manner [1,4]; however, to resolve the clusters at all length scales, extremely fine spatial grids are necessary [4]. Due to computing limitations, the grid size used in simulating industrial scale gas-particle flows is invariably much larger than the length scales of the finer particle clusters. Such a coarse-

grid simulation will clearly not resolve the structures which exist on sub-grid length scales.

Agrawal *et al.* [4] established that the clustered state shows drastically different properties than a uniform field of particles and argued that, in coarse-grid simulations where the fine details of the particle clusters are not resolved, the influence of the sub-grid structures must be accounted for through appropriate sub-grid models. In other words, the TFM must first be coarse-grained [4-7] before it is simulated using coarsely spaced spatial grids. In these coarse-grained equations, the consequences of the flow structures occurring on a scale smaller than a chosen filter width appear through correlations for which closure relations should be derived or postulated.

Adopting the approach pursued in large eddy simulations, one can start with the TFM equations and perform a filtering operation, where the averaging is done over a “filter” length scale which is somewhat larger than the grid size to be used in the coarse-grid simulation of large scale process vessels and over high (temporal) frequencies. The dominant terms in the filtered equations can be recast in exactly the same form as the original TFM equations; however, effective stresses and the interphase interaction force term will now involve additional contributions resulting from the filtering process.

Coarse-graining is achieved in our studies by filtering a kinetic-theory based TFM [4-6]. Andrews *et al.* [6] carried out highly resolved simulations of a kinetic-theory based TFM for gas-particle flows in two-dimensional (2-D) periodic domains, filtered the results and exposed the filter-width dependence of correlations appearing in the filtered equations of motion. The objective of the present study is to examine the filter-width dependence of correlations in the filtered two-fluid model through three-dimensional (3-D) calculations. We will demonstrate that both 2-D and 3-D simulations yield qualitatively similar results.

KINETIC THEORY BASED TWO-FLUID MODEL

In the kinetic theory approach, the continuity and momentum equations for the gas and particle phases are supplemented by an equation describing the evolution of the fluctuation energy (a.k.a. granular energy) associated with the particles, which is used to compute the local granular temperature; the particle phase stress is then expressed in terms of the local particle volume fraction, granular temperature, rate of deformation and particle properties. The kinetic theory model equations and the associated constitutive relations employed in our study can be found in Agrawal *et al.* [4].

We have performed highly resolved 2-D and 3-D simulations of these model equations for a fluidized suspension of particles in large periodic domains, using the MFIX platform [2, 3]. Although the filtering operation does not require a periodic domain, statistical averages can be gathered efficiently from periodic-domain simulations [6]. In each simulation, after an initial transient period which depends on the initial conditions, persistent, time-dependent and spatially inhomogeneous structures develop. Figures 1 and 2 illustrate snapshots of

the particle volume fraction field in 2-D and 3-D systems with domain-average particle volume fraction of 0.05, respectively. The inhomogeneous structures in the 2-D system are in the form of clusters and streamers, whereas those in the 3-D system are globular and filament-like. As shown in these figures, the sizes of the filament-like strands in both systems are of comparable width. The grid resolution used in our simulations was found to yield essentially grid-size independent statistical averages in 2-D simulations, and hence was taken as adequate for 3-D as well.

Using the computational “data” generated through such simulations of the kinetic theory based model equations, we have extracted filtered drag coefficient and particle phase stresses as functions of the local particle volume fraction and the size of the spatial averaging window (i.e. filter size).

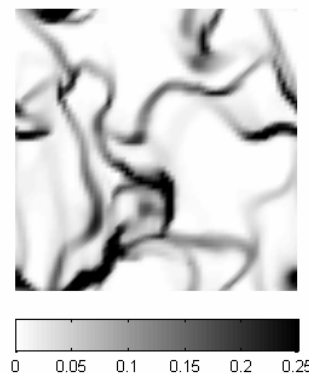


Figure 1: A snapshot of the particle volume fraction field in a large periodic domain of size 16.448 x 16.448 dimensionless units. The domain-average particle volume fraction, $\langle \phi_s \rangle = 0.05$.

In this study, we have performed 2-D and 3-D simulations with domain-average particle volume fractions of 0.05, 0.10, 0.20, and 0.35. Although all our analyses are performed in terms of dimensionless variables, it is useful to present a typical set of dimensional quantities for a system practical interest. See Table 1. These correspond to 75 μm Fluid Catalytic Catalyst particles and ambient air. For the 3-D simulations, we have used a cubic domain of size 16.448 x 16.448 x 16.448 dimensionless units with 64 x 64 x 64 grid points and have compared the filtered quantities for four filter sizes up to 2.056 dimensionless units. These are equivalent to domain and maximum filter size of 8 cm and 1 cm, respectively, for the FCC – ambient air system. The corresponding 2-D simulations were performed in a square domain of size 16.448 x 16.448 dimensionless units with 64 x 64 grid points. The largest 2-D filter size is 2.056 dimensionless units.

As mentioned earlier, we filter the microscopic two-fluid model to average over the small-scale structures that we do not intend to capture in the coarse-grid simulations. For this step, we start with a highly resolved simulation of microscopic two-fluid equations. Initially, we had a homogeneously fluidized system of uniformly sized particles. The system is isothermal, and there are no reactions, which means the energy and species

conservation equations are turned off in the simulation. After an initial transient period depending on the initial conditions, persistent spatially inhomogeneous structures start to form, as shown in figure 1 and 2, and the system reaches a statistical steady state. Filtering, or region averaging, is turned on, which involves volume-weighted averaging the variables necessary for developing the constitutive relationships in regions with sizes ranging from one grid to the domain size. In such a filtering process, the region-averaged (filtered) data are sorted out into bins of filtered particle volume fraction. The filtered quantities were evaluated and averaged within each bin. From such bin statistics, the filtered drag coefficient, filtered particle-phase normal stress, and filtered particle-phase viscosity were calculated as functions of filtered particle-phase volume fraction. In a filtered quantity vs. particle-phase volume fraction plot for various filter sizes,

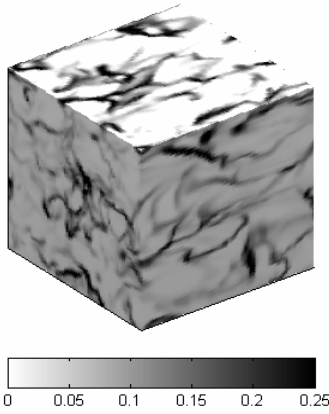


Figure 2: A snapshot of the particle volume fraction field in a large periodic domain of size 16.448 x 16.448 x 16.448 dimensionless units. The domain-average particle volume fraction, $\langle \phi_s \rangle = 0.05$.

each point represents the average of many realizations. These different realizations came from snapshots gathered at various times. To ensure that the snapshots are not too closely correlated, snapshots were gathered only every 50-100 time steps.

d	Particle diameter	7.5×10^{-6} m
ρ_s	Particle density	1500 kg/m ³
ρ_g	Gas density	1.3 kg/m ³
μ_g	Gas viscosity	1.8×10^{-5} kg/m·s
e_p	Coefficient of restitution	0.9
v_t	Terminal settling velocity	0.2184 m/s
$\frac{v_t^2}{g}$	Characteristic length	0.00487 m
$\frac{v_t}{g}$	Characteristic time	0.0223 s

Table 1: Physical properties of gas and solids.

The particle phase momentum equation used in the highly resolved simulations for the particle phase is given in equation 1.

$$\left[\frac{\partial(\rho_s \phi \mathbf{v})}{\partial t} + \nabla \cdot (\rho_s \phi \mathbf{v} \mathbf{v}) \right] = -\nabla \cdot \underline{\underline{\sigma}}_s - \phi \nabla \cdot \underline{\underline{\sigma}}_g + \mathbf{f} + \rho_s \phi \mathbf{g} \quad (1)$$

where ϕ is the volume fraction of particles; \mathbf{v} is the local average velocity of the particle phase; ρ_s is the particle phase density; $\underline{\underline{\sigma}}_s$ and $\underline{\underline{\sigma}}_g$ are the stress tensors associated with the two phases expressed in a compressive sense; \mathbf{f} is the interaction force between the phases per unit volume of the bed; \mathbf{g} is the gravitational acceleration. It is assumed that the gas-particle interaction force, \mathbf{f} , is only due to drag, and the Wen-Yu drag correlation [1] has been used in our simulations. Upon filtering, the momentum equation for the particle phase takes the form given by equation 2.

$$\frac{\partial(\rho_s \overline{\phi \mathbf{v}})}{\partial t} + \nabla \cdot (\rho_s \overline{\phi \mathbf{v} \mathbf{v}}) = -\nabla \cdot \underline{\underline{\Theta}}_s - \overline{\phi \nabla \cdot \underline{\underline{\sigma}}_g} + \underline{\underline{\Psi}} + \rho_s \overline{\phi \mathbf{g}} \quad (2)$$

where $\underline{\underline{\Theta}}_s$ is the filtered particle phase stress; $\underline{\underline{\Psi}}$ is the filtered drag; $\overline{\mathbf{v}}$ is the filtered (region-averaged) particle-phase velocity. The filtered velocities for the particle and gas phases are given in equations 3 and 4.

$$\overline{\mathbf{v}} = \frac{\overline{\langle \phi \mathbf{v} \rangle}}{\overline{\langle \phi \rangle}} \quad (3)$$

$$\overline{\mathbf{u}} = \frac{\overline{\langle (1-\phi) \mathbf{u} \rangle}}{\overline{\langle (1-\phi) \rangle}} \quad (4)$$

The filtered particle phase stress represented in equation 5 involves the filtered particle phase stress from the kinetic theory and the Reynolds stress term; similarly the filtered drag given in equation 6 involves the average of the drag in the original particle phase momentum balance plus the term involving gas pressure fluctuation.

$$\underline{\underline{\Theta}}_s = \underline{\underline{\sigma}}_s + (\rho_s \overline{\phi \mathbf{v}' \mathbf{v}'}) \quad (5)$$

$$\underline{\underline{\Psi}} = \mathbf{f} - \overline{\phi \nabla \cdot \underline{\underline{\sigma}}_g} \quad (6)$$

Here, $\mathbf{v}' = \mathbf{v} - \langle \mathbf{v} \rangle$, where angle bracket denotes average over the filter region and $\langle \mathbf{v} \rangle$ is the volume-weighted particle phase velocity in the filtered region.

$$\langle \mathbf{v} \rangle = \frac{\langle \phi \mathbf{v} \rangle}{\langle \phi \rangle} \quad (7)$$

$$\langle \mathbf{u} \rangle = \frac{\langle (1-\phi) \mathbf{u} \rangle}{\langle (1-\phi) \rangle} \quad (8)$$

$\overline{\mathbf{v}}$ is the ensemble average of $\langle \mathbf{v} \rangle$ over many realizations. Similarly, $\overline{\mathbf{u}}$ is the ensemble average of the volume-weighted gas velocity in the filtered region, $\langle \mathbf{u} \rangle$.

For $\underline{\Theta}_s$ and Ψ we seek simple constitutive models of the form:

$$\underline{\Theta}_s = \overline{\overline{\mathbf{P}}_{s,filtered}} - 2\overline{\overline{\mu}}_{s,filtered} \underline{\mathbf{d}} \quad (9)$$

$$\Psi = \overline{\overline{\beta}}_{filtered} (\mathbf{u} - \mathbf{v}) \quad (10)$$

Each realization of the filtered drag coefficient is thus evaluated through the following averaging over the filtering region. Here the y-direction is pointing vertically up.

$$\beta_{filtered} = \frac{\langle \beta (\mathbf{u}_y - \mathbf{v}_y) \rangle - \langle \phi \left(\frac{dP_g}{dy} \right) \rangle + \langle \phi \rangle \cdot \langle \frac{dP_g}{dy} \rangle}{\frac{\langle (1-\phi) \mathbf{u}_y \rangle}{\langle (1-\phi) \rangle} - \frac{\langle \phi \mathbf{v}_y \rangle}{\langle \phi \rangle}} \quad (11)$$

$\overline{\overline{\beta}}_{filtered}$ is then found by averaging $\beta_{filtered}$ over many realizations.

The new drag Ψ is now defined as the product of a filtered drag coefficient (see Equation 11) and the filtered slip velocity. It should be noted that the filtered drag coefficient for a filter size equal to the grid size corresponds to the original Wen & Yu drag coefficient used in our highly resolved computations.

The filtered particle-phase horizontal normal stress and viscosity given in equations 12 and 13, respectively, include the pressure arising from the streaming and collisional parts captured by the kinetic theory and the sub-filter-scale Reynolds-stress like velocity fluctuations. The filtered particle-phase horizontal stress for a filter size equal to a grid size corresponds to the kinetic theory pressure. Similarly, the filtered particle-phase viscosity for a filter size of one grid point corresponds to the kinetic theory viscosity.

$$\overline{\overline{P}}_{s,filtered,xx} = \overline{\overline{\rho}}_s \overline{\overline{\phi}} \overline{\overline{v'_x v'_x}} + \overline{\overline{P}}_{s,kinetic} = \left[\overline{\overline{\rho}}_s \langle \phi v_x v_x \rangle \right] - \overline{\overline{\rho}}_s \left[\frac{\langle \phi v_x \rangle \langle \phi v_x \rangle}{\langle \phi \rangle} \right] + \left[\overline{\overline{P}}_{s,kinetic} \right] \quad (12)$$

$$\overline{\overline{\mu}}_{s,filtered,xy} = \overline{\overline{\rho}}_s \left[\frac{\langle \phi v_x v_y \rangle - \frac{\langle \phi v_x \rangle \langle \phi v_y \rangle}{\langle \phi \rangle}}{\left[\langle \frac{\partial v_x}{\partial y} \rangle + \langle \frac{\partial v_y}{\partial x} \rangle \right]} \right] + \left[\overline{\overline{\mu}}_{s,kinetic} \right] \quad (13)$$

where square bracket denotes the ensemble average of the volume-weighted quantities in the filtered region.

The filtered particle-phase horizontal normal stress and viscosity described below have been made dimensionless using particle density, terminal velocity and acceleration due to gravity as characteristic density, velocity and acceleration. It should be kept in mind that the trends

discussed in this study with respect to volume fraction apply for the range of volume fractions shown in the corresponding figures.

Filtered Drag Coefficient

In the limit of Stokes drag and no hydrodynamic interaction between particles, the drag coefficient would be $18\mu_g \phi / d^2$. We define dimensionless filtered drag coefficient as $\overline{\overline{\beta}}_{filtered} d^2 / 18\mu_g \phi$.

In Figures 3 and 4 the dimensionless filtered drag coefficient for 2-D and 3-D systems are presented as functions of particle volume fraction for four filter sizes used in the analysis. The filtered particle-phase drag coefficients extracted from 2-D and 3-D simulations manifest qualitatively similar dependence on filter size and particle-phase volume. For a given region size, the filtered drag coefficient initially decreases with increasing particle-phase volume fraction. This is due to the organization of particles into clusters result in an increase in the drag coefficient. We also see that the filtered drag coefficient decreases with region size in both regions. The explanation for this trend is that the larger region sizes will contain larger particle clusters and offer greater

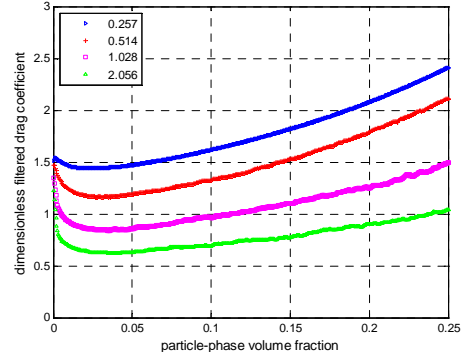


Figure 3: The dimensionless filtered drag coefficient calculated by filtering data gathered from 2-D simulations. The filtered drag coefficients were calculated for various filter sizes, listed in the legend in dimensionless units. Data used for filtering were generated by running simulations for domain-average particle volume fractions of 0.05, 0.10, 0.20, and 0.35.

opportunities for the gas to bypass through. It is clear from the figures 3 and 4, the filtered drag coefficient from the 3-D case is lower for a given filter size than that from the 2-D case. This result was also expected since 3-D inhomogeneous structures, in the form of 3-D globular and filaments (see Figure 1), allow the gas bypass these structures more than the 2-D clusters and streamers (see Figure 2), which take the form of cylinders and sheets if extended to 3-D.

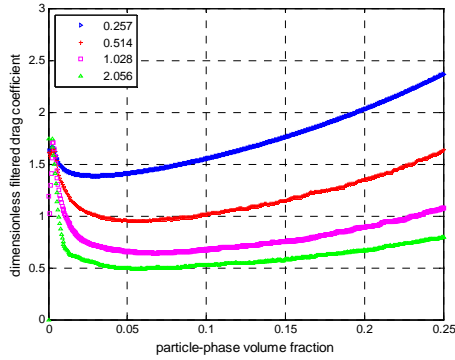


Figure 4: The dimensionless filtered drag coefficient calculated by filtering data gathered from 3-D simulations. Everything else is as in figure 3.

Filtered Particle-phase Horizontal Normal Stress

The filtered particle-phase horizontal normal stresses extracted from 2-D and 3-D simulations manifest similar trends over the range of volume fractions presented in Figures 5 and 6. However, the horizontal stress in 3-D is noticeably smaller than that in 2D. The difference is pronounced for larger filter sizes. Both Figures 5 and 6 illustrate that the filtered particle-phase horizontal normal stress is dependent on the local particle volume fraction and the filter size. The filtered particle phase normal stresses increase as the filter size is increased for a given volume fraction. It is also clear from the figures that the sub-filter-scale stress is significantly larger than that captured by the kinetic theory for both 2-D and 3-D cases. In Figures 5 and 6, the filtered horizontal normal stress for a filter size equal to the grid size corresponds to the kinetic theory pressure.

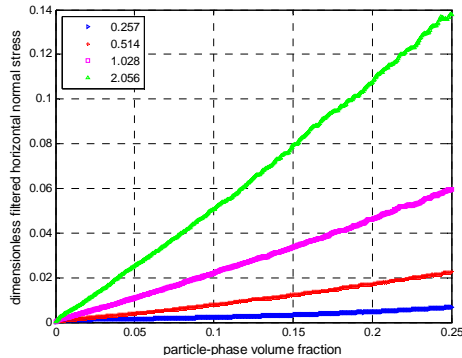


Figure 5: Dimensionless filtered horizontal normal stress for different dimensionless filter sizes, extracted from 2-D simulations.

Filtered Particle-phase Viscosity

Figures 7 and 8 illustrate the dependence of the filtered viscosity on the filter size used in this analysis and local particle volume fraction in 2D and 3D systems, respectively. The filtered particle-phase viscosity extracted from 2-D and 3-D simulations also manifest similar trends, and they are qualitatively comparable over

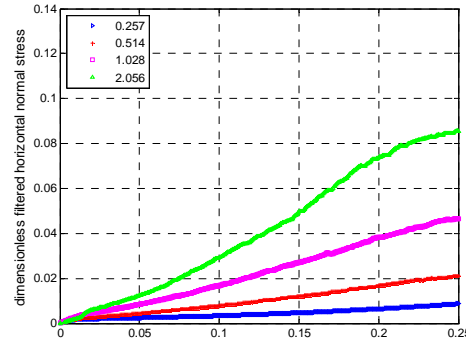


Figure 6: Dimensionless filtered horizontal normal stress for different dimensionless filter sizes, extracted from 3-D simulations.

the range of volume fractions presented in the figures. In both 2-D and 3-D cases the filtered particle-phase

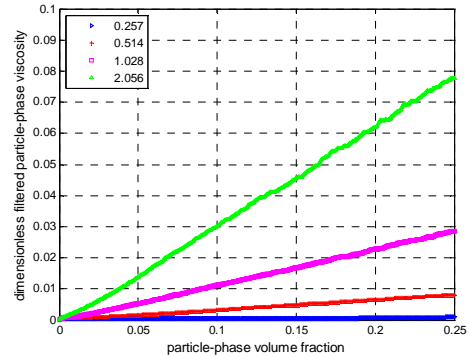


Figure 7: Dimensionless filtered particle-phase viscosity for different dimensionless filter sizes, extracted from 2-D simulations.

viscosity increases with the filter size. It should also be noted that the sub-filter scale viscosity is significantly larger than that captured by the kinetic theory. In Figures 7 and 8, the filtered viscosity for a filter size equal to the grid size corresponds to the kinetic theory viscosity. The sub-filter fluctuations cause the system to be more dissipative on the macro-scale.

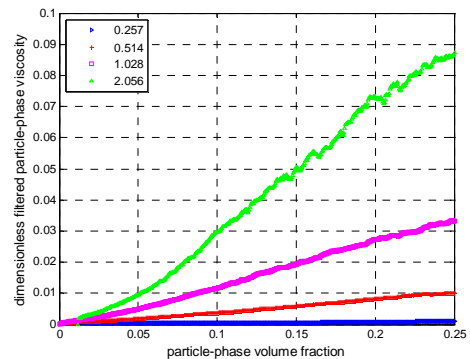


Figure 8: Dimensionless filtered particle-phase viscosity for different dimensionless filter sizes, extracted from 3-D simulations.

SUMMARY

The filtered drag coefficient extracted from the analysis of computational data generated through highly resolved 3-D simulations of a kinetic theory based two-fluid model decreased systematically with increasing filter width. This behaviour is consistent with what was seen earlier in 2-D simulations. The filtered particle-phase stresses extracted from 2-D and 3-D simulations manifest similar trends. Thus, the differences between 2-D and 3-D simulations are not qualitative.

This is in marked contrast to what one observes in single phase turbulence. This difference between two-phase and single phase systems is not surprising, at least in retrospect. The energy to sustain the fluctuations motion in the gas-particle flows is extracted from mean flow via the drag force, which is included in both 2-D and 3-D simulations. Hence the addition of a third dimension makes only a small (but not qualitative) difference to the filtered quantities.

ACKNOWLEDGEMENTS

This work was funded by the grants from the ExxonMobil Research & Engineering Company and the US Department of Energy (DE-PS26-05NT42472-11) to SS.

REFERENCES

- AGRAWAL, K., LOEZOS, P. N., SYAMLAL, M. and SUNDARESAN, S., (2001), "The role of meso-scale structures in rapid gas-solid flows", *J. Fluid Mech.* **445**, 151 – 185.
- ANDREWS, A.T. IV, LOEZOS, P. N. and SUNDARESAN, S., (2005), "Coarse-grid Simulation of Gas-Particle Flows in Vertical Risers", *Ind. Eng. Chem. Res.*, **44**, 6022 – 6037 (2005).
- ANDREWS, A. T. IV, IGCI, Y. and SUNDARESAN, S., (2005), Paper presented at the AIChE Annual Meeting, Cincinnati, November; manuscript under preparation.
- GIDASPOW, D., (1994), *Multiphase Flow and Fluidization*, Academic Press, CA. 31-58, 197 – 238.
- SYAMLAL, M., ROGERS, W. and O'BRIEN, T. J., (1993), *MFIX Documentation*, U.S. Department of Energy, Federal Energy Technology Center, Morgantown, WV, USA.
- SYAMLAL, M., (1998), *MFIX Documentation: Numerical Techniques*, DOE/MC-31346-5824. NTIS/DE98002029.
- ZHANG, D. Z. and VANDERHEYDEN, W. B., (2002), "The effects of mesoscale structures on the macroscopic momentum equations for two-phase flows", *Int. J. Multiphase Flow.* **28**, 805 – 822.